Rotor-floater-mooring coupled dynamic analysis of mono-column-TLP-type FOWT (Floating Offshore Wind Turbine)

Y.H. Bae[*1] and M.H. Kim[2a]

[1]*Texas A&M University, College Station, TX, USA*
[2]*Civil Engineering, Texas A&M University, College Station, TX, USA*

Abstract.   Increasing numbers of floating offshore wind turbines are planned and designed these days due to their high potential in massive generation of clean energy from water depth deeper than 50 m. In the present study, a numerical prediction tool has been developed for the fully-coupled dynamic analysis of FOWTs in time domain including aero-blade-tower dynamics and control, mooring dynamics, and platform motions. In particular, the focus of the present study is paid to the dynamic coupling between the rotor and floater and the coupled case is compared against the uncoupled case so that their dynamic coupling effects can be identified. For this purpose, a mono-column mini TLP with 1.5MW turbine for 80m water depth is selected as an example. The time histories and spectra of the FOWT motions and accelerations as well as tether top-tensions are presented for the given collinear wind-wave condition. When compared with the uncoupled analysis, both standard deviations and maximum values of the floater-responses/tower-accelerations and tether tensions are appreciably increased as a result of the rotor-floater dynamic coupling, which may influence the overall design including fatigue-life estimation especially when larger blades are to be used.

Keywords: renewable wind energy; FOWT (floating offshore wind turbine); rotor-floater-tether coupled dynamics; coupled vs. uncoupled analysis; mono-column mini TLP; tower elasticity; blade control/ aerodynamics; floater responses; tower accelerations; tether tension; fatigue life.

1. Introduction

During the past century, people have been depending on fossil fuels as their major source of energy. However, fossil fuels continue to be depleted and their negative environmental impact is very alarming. Therefore, the importance of increasing the use of clean renewable energy cannot be too much emphasized for the promising future of all human being.

Wind is the fastest growing clean and renewable energy source. Until recently, most of the wind-farm development has been limited to the land space. However, the on-land wind farms also have many negative features, such as lack of available space, noise restriction, shade, visual pollution, limited accessibility in mountainous areas, community opposition, and regulatory problems. Therefore, many countries in Europe started to build wind turbines in coastal waters and so far,

*Corresponding author, PH.D. Student, E-mail: m-kim3@neo.tamu.edu
[a]Professor

most offshore wind farms have been installed in relatively shallow-water areas less than 40-m depth by using bottom-fixed-type base structures.

Recently, several countries started to plan offshore floating wind farms. Although they are considered to be more difficult to design, wind farms in deeper waters are in general less sensitive to space availability, noise restriction, visual pollution, and regulatory problems. They are also exposed to much stronger and steadier wind field to be more effective. Furthermore, in designing those floating wind farms, the existing technology and experience of offshore industry used for petroleum production is directly applicable. In this regard, if technology and infrastructure is fully developed, offshore floating wind farms are expected to produce huge amount of clean electricity at a competitive price compared to other energy sources.

In deeper (>40 m) offshore areas, floating-type wind farms are expected to be more economical than the fixed ones (Tong 1998, Henderson *et al.* 2002, 2004, Musial *et al.* 2003, Wayman *et al.* 2006). Possible disadvantages of floating type wind farms include more transmission loss, the complexity of blade controls due to body motions, larger inertia loading on tall tower caused by greater floater accelerations, and possibly more expensive/complicated installation processes including mooring lines. They are also directly exposed to the open ocean without any natural protection, so they may have to endure harsher environments.

On the other hand, there are also merits of floating base compared to fixed base in the dynamic/structural point of view. In case of fixed OWTs, the high-frequency excitations caused by rotating blades and tower flexibility may cause resonance at system's natural frequencies. This is particularly so as water depth increases, which may significantly shorten its fatigue life. For floating wind turbines, however, their natural frequencies of 6DOF motions are typically much lower than those rotor-induced or tower-flexibility-induced excitations, so the possibility of dynamic resonance with the tower and blades is much less (e.g., Withee 2004, Jonkman *et al.* 2006). One exception is the TLP-type OWT (Bae *et al.* 2010, Jagdale and Ma 2010), which is much stiffer in the vertical-plane modes compared to other floating wind turbines, and thus the effects of such high-frequency excitations from the tower and blades need to be checked. For other types of floating bases with softer mooring system, such as spar or semi-submersible (Roddier *et al.* 2009), the low-frequency excitations related to blade pitch-angle control may cause large-amplitude slowly-varying floater motions. (Nielsen *et al.* 2006) In this regard, the accurate estimation of the coupling effects between the floater dynamics and tower-blade dynamics/control is very important in the optimal design of such floating OWTs.

The present analysis method integrates rotor dynamics and control, aero-dynamics, tower elasticity, floater dynamics, and mooring-line dynamics to investigate the full dynamic coupling among them in time domain. The corresponding rotor-floater-mooring coupled dynamic analysis computer program is developed by combining respective modules. For the floater hydrodynamics, 3D diffraction/radiation panel program WAMIT (Lee *et al.* 1991) was used as a pre-processor for hydrodynamic coefficients. For the dynamics and control of wind blade and tower, the primary design code of wind turbines, FAST, promoted by National Renewable Energy Laboratory (NREL), is employed (Jonkman *et al.* 2004). The portion of the FAST algorithm is implemented into the floater-mooring coupled dynamic analysis program, CHARM3D, and vice versa so that the tower-floater coupling can accurately be achieved. The CHARM3D program has been developed by authors' group to analyze the coupling effects between floating platforms and mooring/riser system (e.g., Kim *et al.* 2001, Arcandra and Kim 2003, Yang and Kim 2010). The CHARM3D program has been verified through numerous comparisons against experiments and field data during the past decade. In this paper, the developed fully coupled dynamic analysis program is applied to a mono-

column 4-leg mini-TLP-type floating OWT designed for 80-m water depth.

2. Numerical analysis of floating offshore wind turbine in time domain

The rotor-floater-tether-fully-coupled time-domain-analysis tool is developed in this study. In order to couple the wind-turbine elastic motion and tether/floater dynamics, two different analysis modules, CHARM3D and FAST, are combined and utilized. The hydrodynamic coefficients including added mass, radiation damping, wave forces, and mean drift forces of floating wind turbine are obtained by a 3D diffraction/radiation preprocessor WAMIT in frequency domain and the information is transferred to the ensuing time-domain-analysis tool, CHARM3D. The mooring dynamics coupled with hull motions are solved at each time step by a generalized-coordinate-based FEM program using high-order element, the details of which are given in Kim *et al*. (1999).

The equation of motion in time domain can be expressed as follows

$$[M + M^a(\infty)]\ddot{\xi} + K\xi = F_1(t) + F_c(t, \dot{\xi}) + F_n(t, \dot{\xi}) + F_m(t) \tag{1}$$

where $M^a(\infty)$ denotes added mass at infinite frequency, $F_I(t)$ is wave exciting force, K=hydrostatic coefficients, $F_n(t, \dot{\xi})$ is nonlinear drag force from Morison's equation, $F_m(t)$=mooring force, and $F_c(t, \dot{\xi})$ radiation force including convolution integral as follows

$$F_c(t, \dot{\xi}) = -\int_{-\infty}^{t} R(t - \tau)\dot{\xi}(\tau)d\tau \tag{2}$$

where ξ, $\dot{\xi}$, and $\ddot{\xi}$ represent the six-degree-of-freedom displacements, velocities, and accelerations of a floating body. The retardation function $R(t)$ is given by

$$R(t) = \frac{2}{\pi}\int_{0}^{\infty} b(\omega)cos(\omega t)d\omega \tag{3}$$

in which b is the linear radiation damping matrix.

The complete nonlinear aero-elastic equations of motion for the wind turbine is

$$M(\underline{q}, \underline{u}, t)\ddot{q} + f(\underline{q}, \dot{\underline{q}}, \underline{u}, \underline{u}_d, t) = 0 \tag{4}$$

where M is the mass matrix, f is the forcing function, $\underline{u}$ and $\underline{u}_d$ are the set of wind turbine control inputs and wind inputs, respectively. The column vectors $\underline{q}$, $\dot{\underline{q}}$, and $\ddot{q}$ are wind turbine motions, velocities, and accelerations. The upper dots mean time derivative and t is time. The details of the dynamic modeling of the tower and blade as well as the applied blade-pitch-angle-control scheme are given, for example, in Jonkman *et al*. (2004).

The wind-turbine dynamics including 6 DOF of platform dynamics are computed simultaneously in a combined matrix by FAST, which is developed by NREL. In the mean time, the CHARM3D calculates all of the external forces acting on the platform at each time step. The CHARM3D feeds the external forces to FAST, then FAST fills out the forcing function in Eq.(4) by using the forces from CHARM3D. The external forces calculated by CHARM3D include 1st-order and 2nd-order (if applicable) wave forces, wave radiation damping forces, nonlinear viscous drag forces from the Morison members, and restoring forces from mooring lines.

The time-varying mooring restoring forces on the floater can be obtained from the top tension of each mooring line and their directional cosines at the connection. Then FAST solves the combined equations of motions including 6-DOF platform motions and all the remaining degrees of freedom of floating-wind-turbine system. Those updated platform kinematics data including all the displacements, velocities, and accelerations are then used in CHARM3D side to get updated external forces. The updated external forces then will be fed into FAST again at the next time step. In doing the coupling between the two modules, FAST and CHARM3D, the coupling time step is not necessarily the same as individual time steps. In general, the FAST time step is smaller than the CHARM3D time step in that the FAST has to solve the tower-blade elastic dynamics, whose natural frequencies are typically high. In the present case, the time step of CHARM3D side is 0.01s and the internal time step for FAST part is 0.005s, which means that at every time interval of 0.01 second, the FAST internally marches 2 steps, and then returns the resultant data to CHARM3D. If the mooring-stiffness of a floating body is softer than that of TLP, like spar or semi-submersible, the coupling time interval can be increased further to make the computational scheme more time efficient without sacrificing overall accuracy. The basic concept of coupling is schematically shown in Fig. 1.

2.1 Specification of wind turbine

The wind turbine analyzed in this study is obtained from the NREL. The model is 1.5-MW-capacity flexible type wind turbine with variable speed & pitch controller. The details of the employed floating wind turbine are summarized in Table 1 and Table 2. The rated power is 1.5 MW, and the rotor diameter is 70 m. The characteristics of the tethers of the TLP are tabulated in Table 3. The flexibility of tower is included by using a linear modal representation as suggested in FAST. As shown in Fig. 2, two lowest fore-aft (and two side-to-side) mode shapes of the tower and
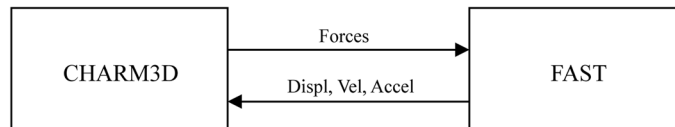

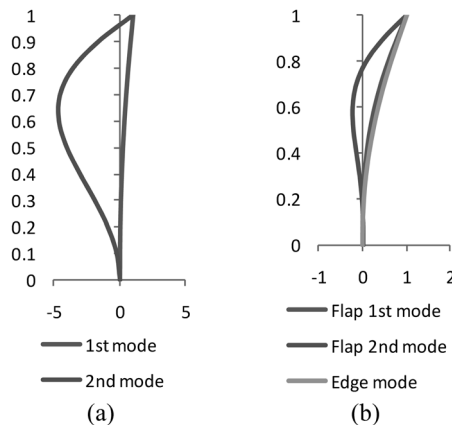Fig. 1 Basic concept of CHARM3D-FAST hybrid model

Fig. 2 Normalized mode shapes of (a) tower and (b) blades

two lowest flap-wise modes and one edgewise mode of the blades are used for coupled dynamic analysis. The corresponding natural frequencies of the tower and blade are tabulated in Table 4.

Table 1 Characteristics of the wind turbine

Blade Mass	11,756 kg
Nacelle Mass	51,200 kg
Hub Mass	15,100 kg
Tower Mass	123,003 kg
Hub Height	84.29 m
Rotor Diameter	70 m
Number of Blades	3
Initial Rotor Speed	20 rpm

Table 2 Characteristics of the floating body

Cylinder Diameter	10 m
Cylinder Height	12 m
Cylinder draft	17 m
Steel Thickness	0.0253 m
Floater Mass	210,435 kg
Buoyant Mass	1,308,687 kg
Center of Gravity	-13.82 m
Center of Buoyancy	-10.89 m
Spoke length/width/height	20/1/1 m

Table 3 Characteristics of the tethers

Number of tether (per spoke)	1
Pretension of tether	2.2E6 N
Diameter of tether	0.0985 m
Axial stiffness (EA)	8.88E8 N

Table 4 Natural frequencies of tower and blade for fixed base

1st tower fore-aft mode	2.59 rad/s
2nd tower fore-aft mode	16.94 rad/s
1st tower side-to-side mode	2.58 rad/s
2nd tower side-to-side mode	16.11 rad/s
Blade 1st flapwise	8.22 rad/s
Blade 2nd flapwise	23.65 rad/s
Blade 1st edgewise	11.83 rad/s

Using this NREL wind turbine model, rotor-floater coupled dynamic analysis in time domain is carried out in 80 m water depth for the given wind-wave-current environment.

2.2 Hydrodynamic coefficients in frequency domain

Wave forces and hydrodynamic coefficients for the submerged body portion are calculated by using the potential-based 3D diffraction/radiation theory. Fig. 3 shows the discretized panel distribution of the floater. The submerged body is X and Y axis symmetric and each one quarter side has 984 panels. Second-order mean drift forces are also calculated so that it can generate slowly-varying drift forces through Newman's approximation method. The nonlinear viscous drag force of the hull is also estimated by employing various Morison members in the time-domain simulations. High modulus polyethylene (HMPE) is selected as a material of the tethers. Two different axial AEs of the 4 tethers are considered to see the effects of the tether axial stiffness in the design. Fig. 4 show the surge, heave, and pitch RAOs of the floater with the given tether-axial-stiffness AE and half AE. The surge/sway stiffness can be approximately calculated by using the formula To/l, in which To=total pretension of tethers and l=length of each tendon. The floater has surge natural frequency around 0.33 rad/sec (period=19s), so more vulnerable to long-wave excitations. Since the stiffness in heave direction is much larger than that in surge direction, the heave response is much smaller than the surge response. It is seen that the heave and pitch responses are directly related to the tether axial stiffness and their magnitudes are approximately doubled if the axial stiffness is halved. However, since the surge/sway stiffness is not directly related to tether axial stiffness, they are invariant for different axial stiffness.
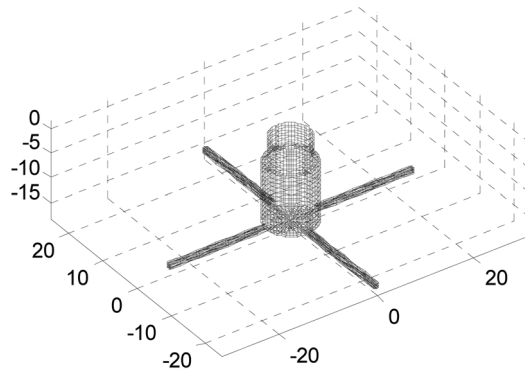

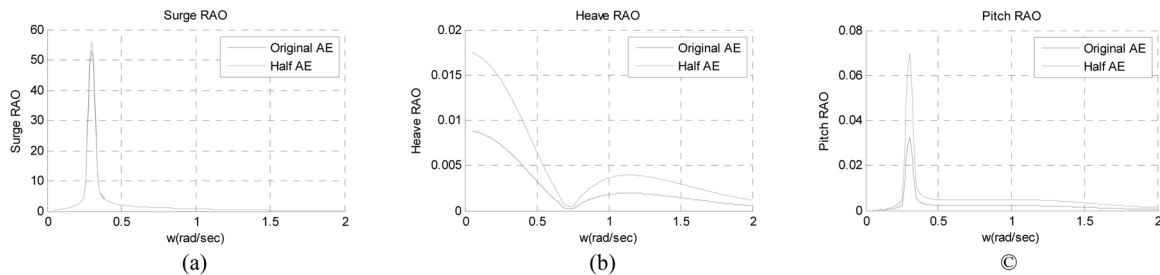Fig. 3 Discretized panel distribution of the submerged portion of the floating body

Fig. 4 (a) Surge, (b) Heave, and (c) Pitch RAOs

Table 5 Natural frequencies of platform motions

Mode	Original AE	Halved AE
Surge/sway (rad/s)	0.33	0.33
Heave (rad/s)	8.35	5.93
Pitch/roll (rad/s)	4.43	3.12

The surge-heave-pitch natural frequencies of the floating body for both original-AE and halved-AE cases are summarized in Table 5. It is seen that the heave-pitch natural frequencies are much higher than typical wave frequencies in both cases, the first-order wave exciting forces cannot cause resonances in vertical-plane motions. Since nonlinear wave-induced viscous drag forces on the hull are also included in the numerical simulations, there still exists a chance of high-frequency excitations but their magnitudes are expected to be small. In the present study, the second-order sum-frequency wave excitations are not included.

2.3 Coupled dynamic analysis of a floating wind turbine in time domain

In this study, the effects of rotating blades, tower flexibility, and blade pitch-angle-control on floater motions and mooring loads are investigated by using the developed time-domain rotor-floater-mooring coupled dynamic analysis program. The rotor-floater coupled analysis model is also compared with the uncoupled analysis model. The coupled analysis is carried out by using CHARM3D-FAST hybrid program, and the rotating blades, flexible tower, and the floater are dynamically interacting to each other at each time step to produce the resultant time histories of respective responses. In the uncoupled dynamic analysis, the effect of rotating blades and their control is not considered and the tower elastic responses are not included either. So, the rotor and tower are considered as rigid part of the whole rigid body. This is the typical case of the dynamic analysis of moored offshore floating oil-production platforms. The wind loading is applied to the swept area of blades with proper drag coefficient to generate similar wind loading as obtained from FAST. For this reason, FAST part is not used and all the platform dynamic/kinematic data are derived by CHARM3D only. The mean wind loading for the uncoupled case is given in Table 7.

The wind and wave headings are collinear and fixed at 0 degree, and the currents do not exist in the present example for convenience. The JONSWAP spectrum is used with significant wave height of 5 m and peak wave period of 8.69s (0.72 rad/s). As for wind, 1-hour mean wind speed (at 10 m height) of 11 m/s is used and time-dependent wind velocities are generated from the corresponding API wind spectrum. The environmental condition is summarized in Table 6.

Table 6 Environmental condition

Reference wind speed at 10m	11 m/s
Mean wind speed at hub height	14.36 m/s
Water depth	80 m
Wave heading	0 deg
Significant wave height	5.0 m
Peak wave period	8.69 sec
Overshooting parameter	2.4

Table 7 Wind load for uncoupled dynamics

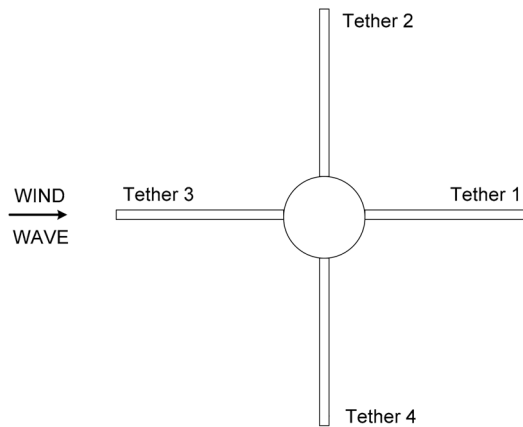|	
Rotor diameter	70 m
Swept area	3848.45 m^2
Drag coefficient	0.332
Uncoupled mean wind load on blades	160.0 kN

Fig. 5 Top-view of cylinder and spokes

4 tethers are modeled as finite elements and each tether has 10 high-order elements. The details of the higher-order finite-element modeling in general coordinate for mooring lines and risers are given in Kim *et al*. (2001a). In the rotor-floater-mooring coupled dynamic analysis, the updated position of the platform solved by FAST at every time step will be a new boundary condition at the ends of tethers, and the ensuing mooring dynamics for the given condition are solved in CHARM3D side to find the updated top tension and its directional cosines. This information is then transferred to FAST side.

During the time-marching procedure, several control methods are also working to maximize and optimize the power capture. In this study, blade-pitch-control and variable-speed-torque-control methods are adopted. The blade-pitch control model is the WindPACT 15A1001 (Jonkman *et al*. 2005) and the pitch angle is determined by measured shaft speed. The pitch angle varies from 2.6 deg to 90 deg to maintain proper shaft speed. The variable-speed-torque-control model used in this analysis is the simplified model that is operated by pre-defined parametric speed-torque curve. Other control methods, such as HSS brake control and nacelle yaw control, are not used in this example for simplicity.

3. Numerical results and discussions

The 6-DOF motions and tether-top tensions from the coupled and uncoupled dynamic analyses are compared to observe the effects of rotor-tower dynamic coupling. Due to the symmetry of the hull geometry and the direction of wind and wave, the sway, roll, and yaw motions of the uncoupled case are zeros. However, the sway, roll, and yaw motions of the coupled case show non-zero

displacements because of the dynamic interactions (aero-dynamic loading, rotating inertia, gyro effects etc.) between the hull and wind turbine. The transverse loading for sway-roll-yaw comes from the aero-dynamic loading from blades while rotating. The resonance amplitudes of surge and sway at their natural frequencies (0.35 rad/s) are greater in the coupled case due to the additional disturbance from the tower and wind blades. Since the system is very stiff in heave mode, the heave amplitudes are mostly caused by set-down effects due to surge motions.

The time histories of tether-top tensions and the corresponding spectra are plotted in Figs. 12-15.
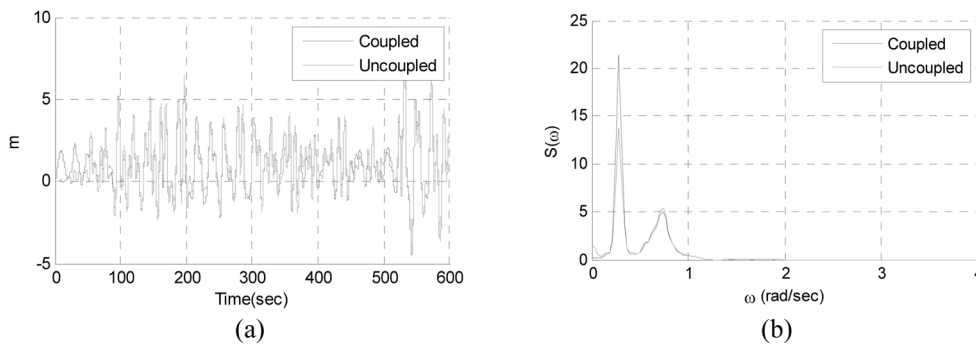
Fig. 6 Time histories (a) and spectra (b) of the surge motion
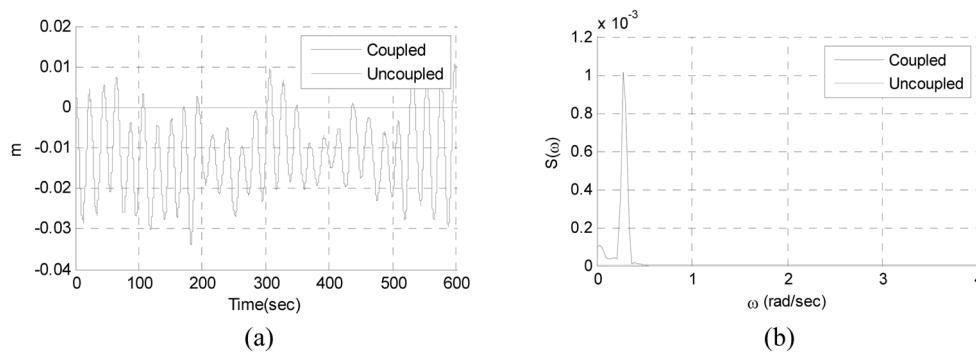
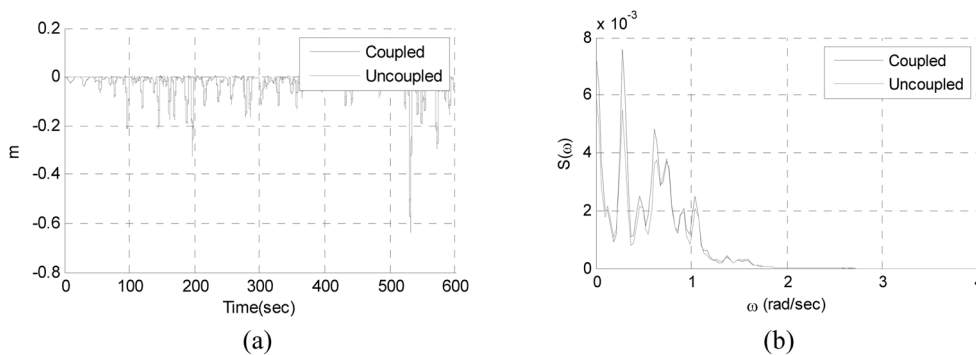Fig. 7 Time histories (a) and spectra (b) of the sway motion

Fig. 8 Time histories (a) and spectra (b) of the heave motion
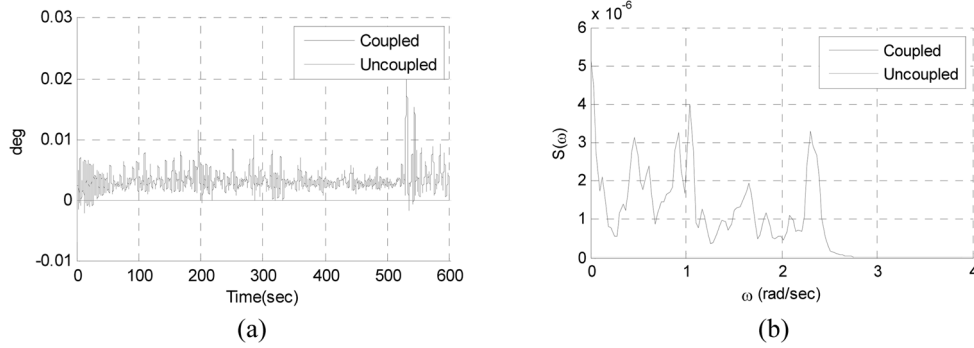
Fig. 9 Time histories (a) and spectra (b) of the roll motion
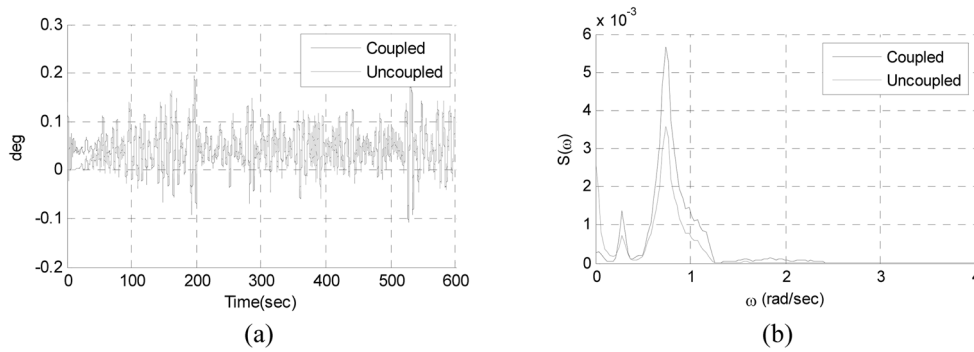

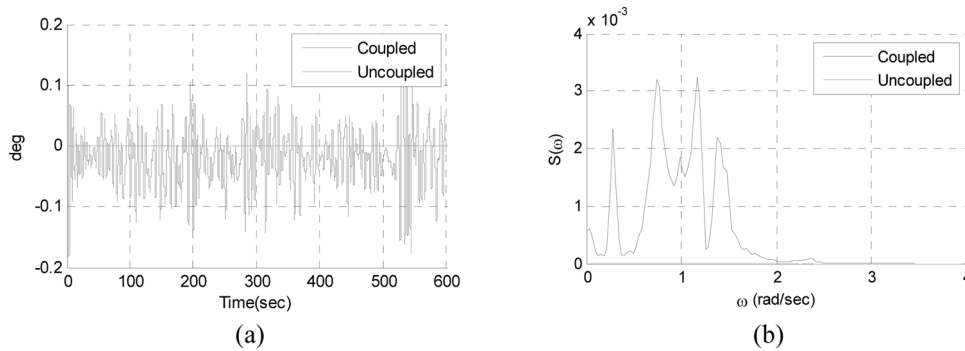Fig. 10 Time histories (a) and spectra (b) of the pitch motion

Fig. 11 Time histories (a) and spectra (b) of the yaw motion

The top tensions of tether 1 and 3 are mostly affected by pitch motions, so their spectral shape resembles that of pitch motion. The top tensions of tether 2 and 4 are dependent upon the roll motion of the hull, and the roll motion is also affected by transverse aerodynamic loading and tower elasticity. This coupling effect can be seen by the peaks around 2.33 rad/s in Figs. 13(b) and 15(b), which is close to the lowest side-to-side tower bending mode. This kind of coupling effect cannot be observed in the uncoupled analysis. The lowest bending mode of the same land-based wind turbine is about 2.58 rad/s that is slightly higher than the actual peak of the mini-TLP-based turbine.

The TLP floater attached under the tower base acts as a soft foundation and may reduce the overall stiffness of the whole system compared to the case of land-based tower. As a result, the lowest tower-bending-mode natural frequency is shifted to lower position. If the roll/pitch natural frequency is close to that of the lowest tower-banding mode, more significant resonance effects could be observed.

Table 8 shows the statistics of the 6-DOF floater motions in 80 m water depth. The noticeable increases of standard deviations of coupled sway/roll/yaw motions compared to uncoupled motions
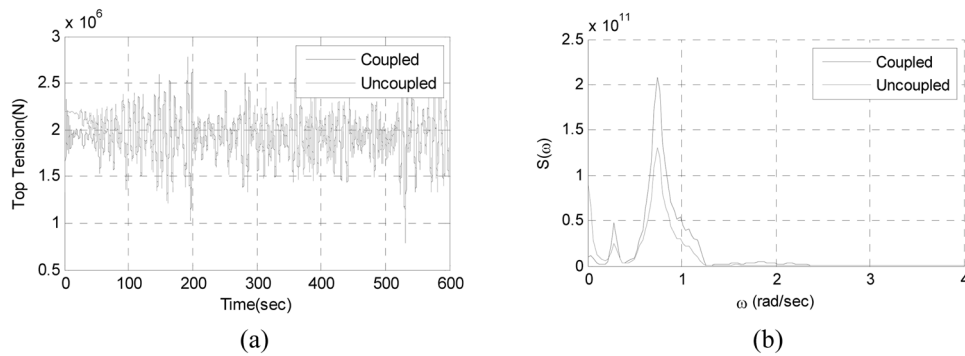

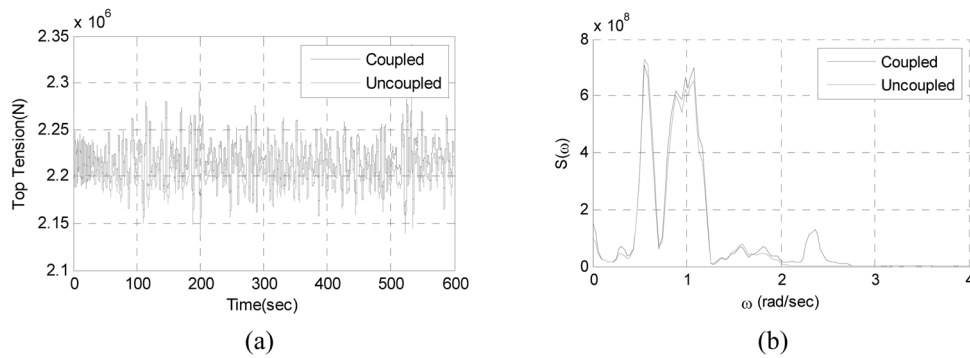Fig. 12 Top tension time histories (a) and spectra (b) of tether 1

Fig. 13 Top tension time histories (a) and spectra (b) of tether 2
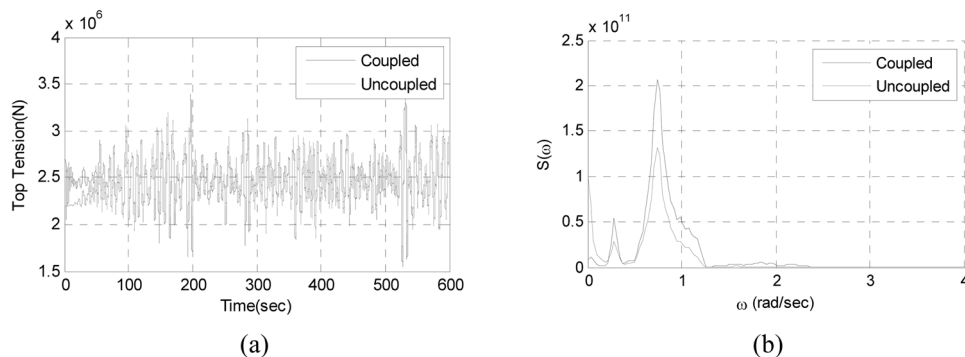

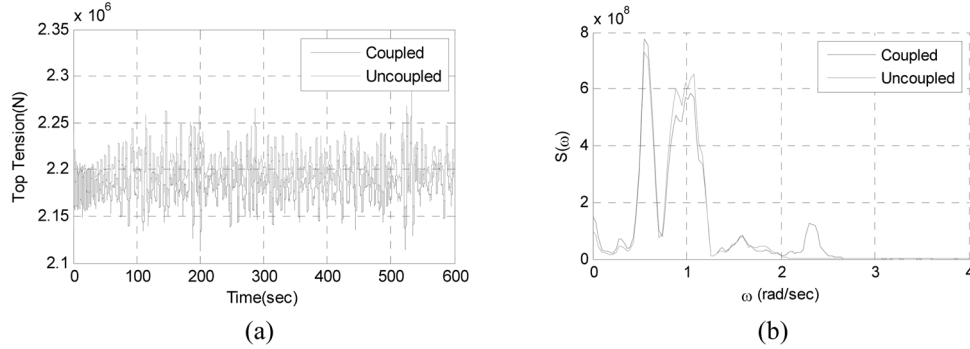Fig. 14 Top tension time histories (a) and spectra (b) of tether 3

Fig. 15 Top tension time histories (a) and spectra (b) of tether 4

represent the effect of rotor-floater dynamic coupling. In addition, due to the rotor-floater dynamic coupling, all the maximum values are increased except heave. In particular, the maximum pitch amplitude is increased by 21% after including rotor-floater dynamic coupling.

The differences in hull motions between the coupled and uncoupled cases directly affect the top-tension statistics of tethers, which are summarized in Table 9. Note that the standard deviations of tether-tension for tether 1 and 3 are increased by 14~15% and it directly affects the maximum tension to be increased by 7% compared to the uncoupled-analysis case. Those differences are expected to increase as the size of wind turbine increases that will result in more rotor-floater dynamic coupling.

Fore-aft accelerations at 3 different locations of the tower are also investigated and the coupled and uncoupled cases are compared. For the coupled case, the total acceleration at a given height is calculated by the summation of the local tower acceleration from elastic vibration and the global acceleration due to the hull motion. Phase differences between the local tower acceleration and

Table 8 Floater-motion statistics (UC: Uncoupled, C: Coupled)

		Max.	Min	Mean	SD
Surge (m)	UC	8.43E+00	-3.85E+00	1.01E+00	1.62E+00
	C	9.02E+00	-4.50E+00	1.08E+00	1.72E+00
Sway (m)	UC	1.23E-06	-1.13E-06	-8.74E-09	4.65E-07
	C	1.07E-02	-3.40E-02	-1.17E-02	9.50E-03
Heave (m)	UC	6.56E-03	-5.59E-01	-2.59E-02	5.23E-02
	C	5.71E-03	-6.37E-01	-3.02E-02	5.64E-02
Roll (rad)	UC	5.91E-10	-9.00E-10	-1.45E-11	1.21E-10
	C	3.52E-04	-1.20E-04	5.97E-05	3.41E-05
Pitch (rad)	UC	3.47E-03	-1.31E-03	7.49E-04	6.29E-04
	C	4.20E-03	-1.89E-03	7.66E-04	7.19E-04
Yaw (rad)	UC	1.02E-08	-1.02E-08	3.23E-10	2.85E-09
	C	2.41E-03	-3.18E-03	-3.25E-04	7.96E-04

global acceleration are also considered and included in the calculation of the total acceleration. In the uncoupled analysis, the whole system is treated as a rigid body, so only the global accelerations are considered at the respective heights.

The statistics of the tower fore-aft accelerations shows that the maximum acceleration of the coupled analysis is increased by 87~97% compared to the uncoupled case. We have more increase at higher position. This increase is caused not only by the additional tower elastic vibration but also

Table 9 Top-tension statistics (UC: Uncoupled, C: Coupled)

		Max.	Min	Mean	SD
Tether 1 (N)	UC	2.67E+06	1.05E+06	1.94E+06	2.18E+05
	C	2.86E+06	7.84E+05	1.94E+06	2.48E+05
Tether 2 (N)	UC	2.30E+06	2.14E+06	2.20E+06	1.98E+04
	C	2.34E+06	2.15E+06	2.22E+06	2.10E+04
Tether 3 (N)	UC	3.45E+06	1.76E+06	2.46E+06	2.20E+05
	C	3.68E+06	1.55E+06	2.47E+06	2.52E+05
Tether 4 (N)	UC	2.30E+06	2.14E+06	2.20E+06	1.98E+04
	C	2.28E+06	2.11E+06	2.18E+06	2.02E+04

(a)   (b)
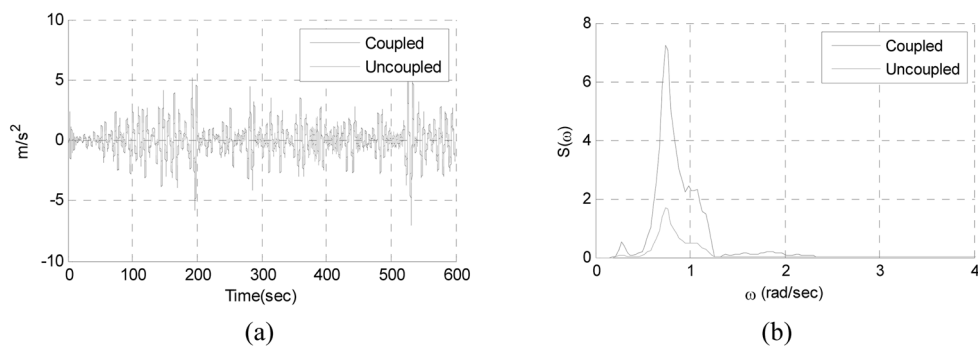
Fig. 16 Tower acceleration time histories (a) and spectra (b) at the height of 78.27 m from MWL

(a)   (b)

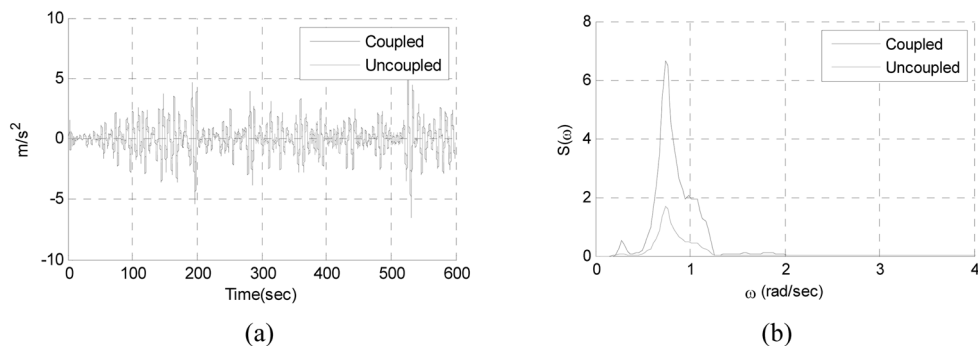Fig. 17 Tower acceleration time histories (a) and spectra (b) at the height of 53.56 m from MWL

(a)   (b)
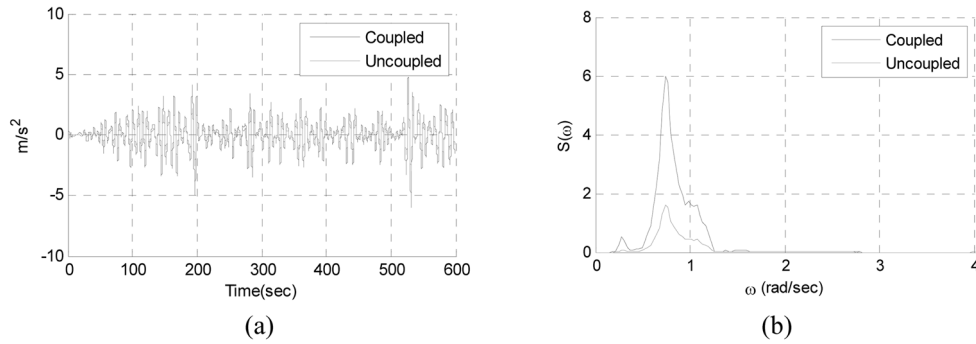
Fig. 18 Tower acceleration time histories (a) and spectra (b) at the height of 4.12 m from MWL

Table 10 Tower acceleration statistics (UC: Uncoupled, C: Coupled)

		Max.	Min	Mean	SD
78.27m from MWL (m/s^2)	UC	3.13E+00	-3.52E+00	-1.24E-03	7.74E-01
	C	6.16E+00	-7.07E+00	-2.72E-03	1.49E+00
53.56m from MWL (m/s^2)	UC	2.93E+00	-3.29E+00	-1.15E-03	7.22E-01
	C	5.49E+00	-6.54E+00	-2.74E-03	1.39E+00
4.12m from MWL (m/s^2)	UC	2.54E+00	-3.02E+00	-9.66E-04	6.63E-01
	C	4.74E+00	-5.99E+00	-2.59E-03	1.29E+00

by the increase of hull motion (especially pitch motion) itself by rotor-floater coupling effects. This means that the uncoupled analysis, which does not include the tower elasticity and aero-floater-rotor dynamic coupling, is not good enough to reasonably estimate the tower accelerations. The accurate estimation of the accelerations is very important since large accelerations may cause fatigue/structural failure through the corresponding inertial loading on various parts of super-structures.

Finally, the effects of softer foundation are investigated by reducing the tether axial stiffness by half. The corresponding change in surge-heave-pitch natural frequencies is summarized in Table 5. If the axial stiffness AE of tethers is reduced by half, we can see more distinct rotor-floater coupling effects. The top-tension spectra of tether 2 and 4 with reduced AE are plotted in Fig. 19. The small peak at 2.33 rad/s is shifted to 2.1 rad/s and its magnitude is greatly amplified as a result of employing softer floater unit. In Table 4, the original lowest banding mode of the tower with fixed bottom is 2.59 rad/s. It is seen that the lowest bending-mode natural frequency shifts toward the lower side as the foundation stiffness decreases, which is another important result of rotor-floater dynamic coupling. In addition to this, the hull heave-pitch-roll natural frequencies are also altered (moving to lower side) with the softer tethers, as indicated in Table 5. In deeper water, the pitch-roll natural frequency may become closer to the lowest-bending natural frequency, and thus the coupling effect between the rotor and hull is expected to increase even more. The pitch acceleration and tower-top acceleration between the AE and half-AE cases are also compared in Fig. 20. As can be intuitively expected, the pitch acceleration for the vertically softer foundation is greater.
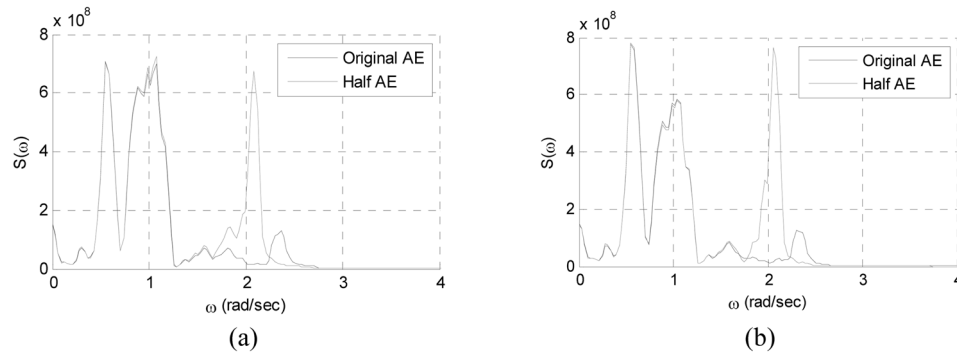
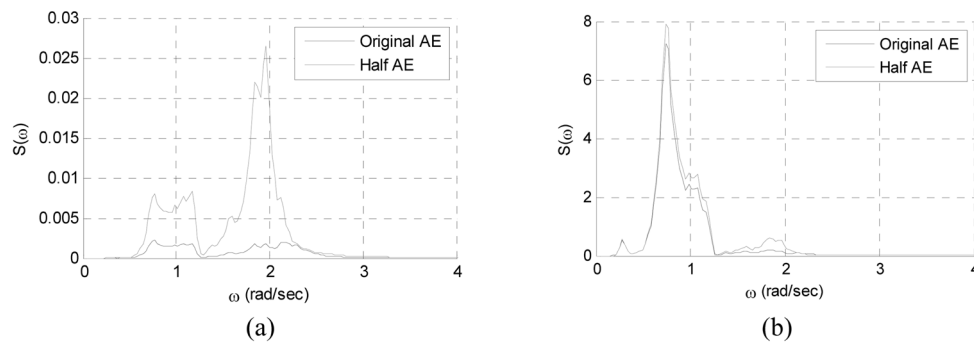Fig. 19 Top-tension spectra of tether2 (a) and tether 4 (b)

Fig. 20 Spectra of hull pitch acceleration (a) and tower-top acceleration (b)

4. Conclusions

In this paper, a mini (mono-column)-TLP-type 1.5MW floating offshore wind turbine that can be used in deeper areas is studied for the water depth of 80m. The newly developed numerical tool can analyze rotor-floater-tether coupled nonlinear dynamics in time domain and was used for the floater-motion, tower-flexible-response, and tether-tension simulations for two different tendon stiffness in a collinear wind-wave environment. The coupled analysis includes rotor and mooring dynamics with elasticity, blade aerodynamics, blade-pitch-angle control, and floater motions as a rigid body. In particular, the dynamic coupling effects between the rotor and floater are investigated by comparing the rotor-floater coupled-analysis results with uncoupled-analysis results through a series of time-domain simulations.

It is seen that the rotor-floater coupling effects increase the standard deviations and maximum values of floater motions and accelerations and tether tensions. Therefore, it is important for both maximum-stress and fatigue-life point of view. In particular, the rotor-floater dynamic coupling significantly increases the resulting accelerations along the tower, which is a great concern for the safety of top structures and their tie-down system. The rotating blades and tower elastic modes produce transverse (sway-roll-yaw) loads and responses despite the symmetry of the system. The rotating blades and tower elastic modes additionally cause high-frequency vibrations. The high frequency excitations are also a concern for the fatigue life of tethers and wind turbines. The rotor-

floater coupling effects are sensitive to the choice of foundation stiffness and expected to increase as blade diameter (or wind velocity) increases. The present methodology is applicable to any types of offshore wind farms with floating foundations.

Acknowledgements

References

Arcandra and Kim, M.H. (2003), "Hull/mooring/riser coupled dynamic analysis and sensitivity study of a tankerbased FPSO", *App.Ocean Res*., **25**, 367-382.

Bae, Y.H., Kim, M.H., and Shin, Y.S. (2010), "Rotor-floater-mooring coupled dynamic analysis of mini-TLP-type offshore floating wind turbines*" Proceedings of the 29th Int. Offshore Mechanics and Arctic Engineering Conference*, Shanghai.

Gilmore J. and Miller J. (2006), Mooring with High Modulus PolyEthylene (HMPE) Fiber lines, Samson Rope Technologies, Ferndale, WA.

Henderson, A.R, Leutz R, and Fujii T. (2002), "Potential for Floating Offshore Wind Energy in Japanese Waters", *Proceedings of the ISOPE conference.*

Henderson, A.R., Bulder, B., Huijsmans, R., Peeringa, J., Pierik, J., Snijders, E., van Hees, M., Wijnants ,G.H. and Wolf, M.J. (2004), "Floating windframs for shallow offshore sites", *Proceedings of the ISOPE conference.*

Jagdale, S. and Ma, Q.W. (2010), "Practical simulation on motions of a TLP-type support structure for offshore wind turbines", *Proceedings of the ISOPE conference*, China.

Jonkman J.M. (2003), Modeling of the UAE wind turbine for refinement of FAST_AD,NREL/TP-500-34755, National Renewable Energy Laboratory, Golden, CO.

Jonkman, J.M and Buhl, Marshall L.B. (2004), FAST user's guide NREL/EL-500-29798, National Renewable Energy Laboratory, Golden, CO.

Jonkman J M, and Sclvounos, P, D. (2006), Development of fully coupled aero elastic and hydrodynamic models for offshore wind turbines, NREL/CP-500-39066, National Renewable Energy Laboratory,Golden,CO.

Kim, M.H., Ran, Z., and Zheng, W. (2001a), "Hull/mooring coupled dynamic analysis of a truss spar in time domain*", Int. J. Offshore Polar Eng.,* **11**(1), 42-54.

Kim, M. H., Tahar, A. and Kim, Y.B. (2001b), "Variability of TLP motion analysis against various design/ methodology parameters"*, Proceedings of the ISOPE'01,* Stavanger, Norway.

Kosugi, A., Ogata, R., Kagemoto, H., Akutsu, Y and Kinoshita, T. (2002), "A feasibility study on a floating wind farm off Japan coast", *Proceedings of the ISOPE conference.*

Lee, C.H., Newman, J.N., Kim, M.H. and Yue, D.K.P. (1991), "The Computation of Second-order Wave Loads",*Proceedings of the 10th OMAE*, Stavanger, Norway.

Musial, W., Butterfield, S. and Boone, A. (2003), Feasibility of floating platform systems for wind turbines", NREL/CP-500-34874, National Renewable Energy Laboratory, Golden, CO.

Nielsen, F.G., Hanson, T.D. and Skaare, B. "Integrated Dynamic analysis of floating offshore wind turbine", *Proceedings of the OMAE 2006-92291*, Germany.

Roddier, D., Cermelli, C. and Weinstein, A. (2009), "Windfloat: a floating foundation for offshore wind turbines Part 1. Design basis and qualification process", *Proceedings of the OMAE Conference,* Honolulu,

Tong, K.C. (1998), "Technical & economic aspects of a floating offshore wind farm, *J. Wind Eng. Ind. Aerod.,* **74-76**, 399-410.

Wayman, E.N., Sclavounos, P.D., Butterfield, S., Jonkman, J. and Musial, W. (2006), Coupled Dynamic Modeling of Floating Wind Turbine Systems, OTC, Houston, TX.

Withee, J.E. (2004), Fully coupled dynamic analysis of a floating wind turbine system, Ph.D. dissertation, department of ocean engineering, massachusetts institute of technology, Cambridge, MA.

World Renewable Energy Congress (2003), Renewable Energy Past, Present, and Future, National Renewable Energy Laboratory, Golden, CO.

Yang, C.K. and Kim, M.H. (2010), "Transient effects of tendon disconnection of a TLP by hull-tendon-riser coupled dynamic analysis", *Ocean Eng.,* **37**(9), 678-687.